SEASAT, ERS-1/2 AND NSCAT SCATTEROMETER-OBSERVED CHANGES ON THE LARGE ICE SHEETS

Mark R. Drinkwater* and David G. Long**

*Jet Propulsion Laboratory, California Institute of Technology
4800 Oak Grove Drive, CA 91109, USA
**Electrical and Computer Engineering Dept., Brigham Young University
Provo, UT 84602, USA

ABSTRACT

Satellite-borne wind scatterometers are effective tools for monitoring ice sheets, and microwave imaging techniques enable comparison of historic and contemporary scatterometer data in climate change studies. We document scattering characteristics of the Greenland and Antarctic ice sheets using data from the NSCAT, ERS-1/2 and Seasat SASS instruments. C- and Ku-band data enable characterization of frequency- and incidence-angle dependent scattering characteristics, together with regional and seasonal melting delineation. NSCAT-SASS data differences indicate 18 year changes in microwave backscattering coefficient in response to decadal time-scale changes in the spatial patterns of ice sheet accumulation and ablation.

1. INTRODUCTION

Controversy over the relationship between global warming and changes in the Greenland ice sheet [Refs. 1, 2] make it imperative to accurately quantify mass balance and the time and space scales of variability in snow accumulation and ablation. Briefly in 1978, and since 1991, microwave radar has been used to study relationships between backscatter characteristics and snow and ice surface structures on temperate glaciers and polar ice-sheets [Refs. 3, 4]. On this basis, satellite microwave radar data have been used on large ice sheets to map the relative size and locations of ice sheet physical zones or 'facies' [Refs. 5, 6].

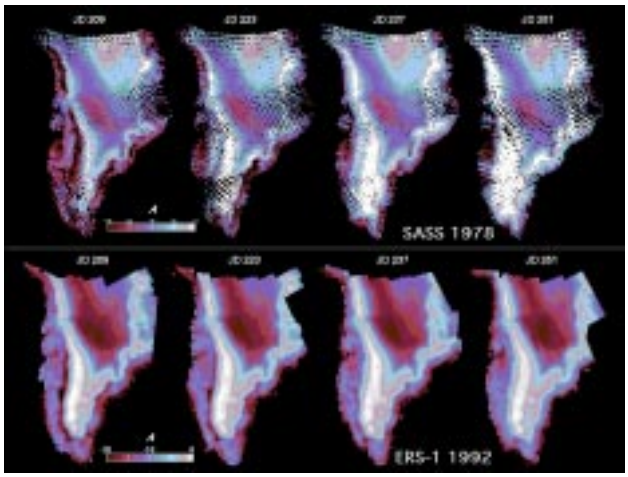

Figure 1. *Greenland time series images generated from 1978 SASS and 1992 ERS-1 scatterometer data for selected days of the year. Colors indicate* $\sigma^{\circ}_{vv}(40°)$ *at Ku- and C-band, respectively.*

Microwave backscattering depends on both the roughness and physical characteristics of the snow and ice [Refs. 7, 8]. For example, liquid water in snow dramatically changes the permittivity and thus its scattering signature. This provides an efficient means of monitoring backscatter changes which accompany diagenetic changes forced by seasonal ablation and/or metamorphic processes. Synthetic aperture radar (SAR) provides high resolution images of ice sheets, but the spatio-temporal coverage of 100 × 100 km SAR images is limited. Scatterometers provide comparatively lower resolution but more frequent coverage, and also measure the backscatter coefficient over a broad range of incidence angles [Ref. 9]. Here we study changes in the Greenland and Antarctic ice sheets using data from the C-band (5.3 GHz) European Space Agency ERS-1 and 2 (EScat) wind scatterometers, NASA's Ku-band (13.6 GHz) scatterometer (NSCAT), and the NASA Seasat scatterometer (SASS).

2. SCATTEROMETER IMAGING OF ICE SHEETS

The EScat wind scatterometer instrument (launched on ERS-1 in July 1991 and ERS-2 in April 1995) measures the vv-polarized normalized radar cross-section σ°_{vv} at various azimuth and incidence angles along a single 500 km-wide swath. EScat acquires these 50 km resolution data on a 25 km grid and has successfully compiled a continuous measurement dataset from 1991 until the present day. The only measurement conflict occurring in the polar regions is that the Scatterometer sub-system of the Active Microwave Instrument (AMI) is periodically switched off during competing high-data-rate SAR-mode operation. This results in some data black-outs in the vicinity of operable Antarctic SAR receiving stations.

The complementary NSCAT sensor was launched in August 1996 aboard the Japanese ADEOS-I satellite. Unfortunately, an untimely failure of the ADEOS platform in June 30, 1997 resulted in a curtailed NSCAT dataset lasting a period of only 10 months - and the loss of a valuable tool for ice studies. NSCAT nonetheless recorded the normalized radar cross-section, σ° (hh- and vv-polarized) while crossing the polar regions several times daily. Measurements at various azimuth and incidence angles were made in hexagonal 25 km resolution cells on a 25 km grid, along two 600 km wide swaths separated by a 400 km wide gap. The Ku-band SASS, from which NSCAT originated, also operated for only 100 days between June 28 and October 10, 1978 before Seasat failed. It made 50 km resolution measurements along two 500 km

swaths on an irregular sampling grid.

Over glacial ice, σ° (dB) is approximately a linear function of θ in the range $20^\circ \bullet \theta \bullet 55^\circ$ [Ref. 5];

$$\sigma^\circ(\theta) = A + B(\theta - 40^\circ) \qquad (1)$$

where the coefficients A and B depend on surface characteristics and polarization. The term A is the'incidence-angle-normalized' backscatter coefficient σ°, at 40°, and B describes its dependence on θ. A and B are both sensitive to snow and ice physical characteristics and surface roughness. The scatterometer image reconstruction algorithm with filtering (SIRF) is used to generate enhanced resolution images of A and B from scatterometer data from Greenland and Antarctica [Refs. 5, 9-11]. Resulting 6-day average images at 3-day intervals are derived as a trade-off between resolution enhancement and temporal averaging. The EScat images have a resolution of approximately 20-25 km and NSCAT images a resolution of around 8-10 km. The resulting ice sheet dataset, comprising 3-daily data, is sampled to the same pixel spacing (8.8 km) and then compared and described in this paper.

3. ICE SHEET BACKSCATTER VARIABILITY

3.1 Greenland

The surface of the Greenland ice sheet is subdivided into 'facies', the boundaries of which are established with respect to extent of melt or ablation influence [Ref. 6]. Within each facies, near-surface snow and ice properties have unique characteristics. At the lowest elevations, summer melting removes the entire annual accumulation of snow to reveal bare glacier ice. The *firn line* delimits the upper margin of this zone, separating it from the 'soaked' facies where saturation of the annual snow layer occurs. The upper limit of soaking is called the *saturation line*. Localized melt-water percolation occurs between this and the upper limit of surface melting, the *dry snow line*. In the 'percolation' facies annual increments of snow are neither completely wetted nor raised to the melting point. Percolation decreases with elevation

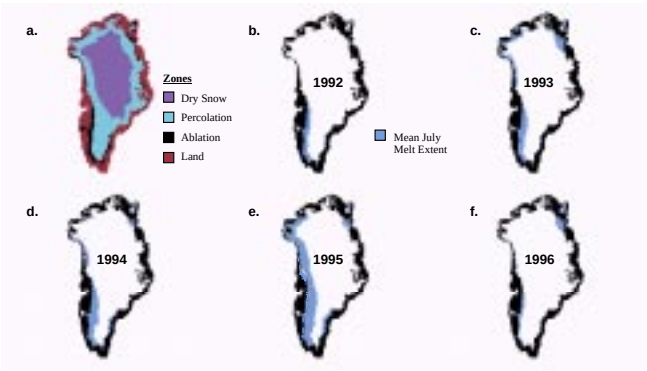

Figure 2. *(a) Greenland snow and ice facies determined from coincident EScat and NSCAT data; and (b)-(f) mean monthly July ice-sheet melt extent from EScat data.*

diminishing to a negligible amount at the lower boundary of the dry snow zone. As glacier facies are not always expressed as strong gradients in surface properties, they are best discerned with microwave measurements which penetrate up to several meters into the surface of the snow and ice [Refs. 5, 8].

Seasonal modulations of σ° in Fig. 1 indicate changes in surface-layer properties in summer. Meltwater alters the surface reflectivity and transmissivity, limiting sub-surface volume scattering effects by increasing absorption and extinction. In addition, σ° is influenced by layering which results from seasonal snow accumulation and melt patterns [Ref. 5]. The spatial extent of summer melt appears as low σ° values around the lower elevation fringe of the ice sheet, particularly on day 209. The surface-melt signature is similar at both frequencies. Differences in melt extent between the upper and lower panels are accounted for by interannual variability in the length and spatial extent of the melt seasons. Typically, melting ceases by day 237, with refreezing then increasing σ° at both frequencies. Monthly mean July melt extent is shown together with the facies in Fig. 2. The

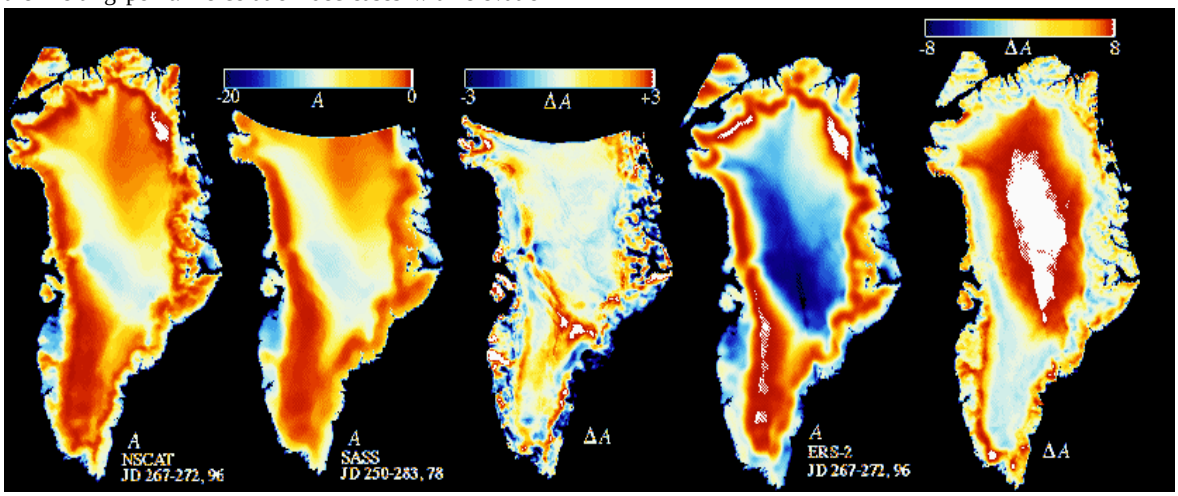

Figure 3. *(a) NSCAT A image for the period 267-272, 1996; (b) SASS A image for days 250-283, 1978; (c) NSCAT-SASS A difference map of Greenland. (d) ERS-2 A image for days 267-272, 1996; and (e) NSCAT - ERS (Ku - C band) A difference image for days 267-272.*

1990's saw two of the smallest (1992: 8.1×10^4 km^2; and 1996: 10.4×10^4 km^2), and perhaps the largest (1995: 25×10^4 km^2) melt extent in the last two decades. Melting in July 1995 is more extensive than at any other time during the satellite data record [2], encroaching upslope upon the dry snow zone along the entire north-western ice-sheet flank. Percolation zone stratigraphic discontinuities and a horizon comprising a high proportion of solid ice in layers, lenses and ice pipes is created as meltwater percolates downwards and refreezes at depth (~1m) [6]. The lower elevation boundary of this zone is clearly indicated in Fig. 1 by a sharp transition between low and extremely high backscatter values. As the surface cools during autumn, the penetration depth increases beyond the depth at which ice lenses form and volume scattering from buried scatterers increases σ° in both Ku- and C-band images to some of the highest known values on earth [7, 8]. Low σ° values in central Greenland are well separated from percolation zone values exceeding -5 dB. Additionally C-band microwaves penetrate dry snow more effectively than Ku-band. Shorter wavelengths are scattered more effectively by snow grains, and thus the Ku-band σ° exceeds C-band values. The frequency difference *A* image (*i.e.* NSCAT-EScat) in Fig. 3(e), and a contour value of 1.8 dB is used to define the lower boundary of the dry-snow zone shown in Fig. 2(a).

Downslope of the firn line, in the saturated facies, horizons are obliterated by the effects of summer melting, reducing winter contrast between the ablation and saturated zones. As a result the two are indistinguishable, and the radar senses only a broad 'ablation zone' [5]. Near the ice sheet margins, the surface

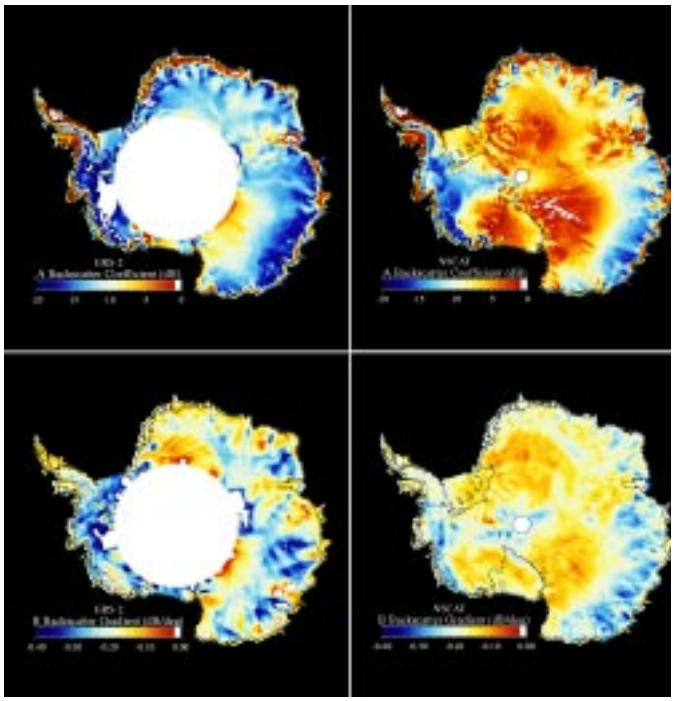

Figure 4. *Mean Antarctic scatterometer ice sheet images for 20-30 September, 1996, for; (a) ERS-2 A values; NSCAT A values; (c) ERS-2 B values; and (d) NSCAT B values.*

autocorrelation function determines *A* and *B* by surface scattering, and the roughness scale causes greater backscattering at Ku-band than C-band of up to 8 dB in Fig. 3(e). Together with the seasonal variations in σ° this is used to define the 1996 extent of the ablation zone in Fig. 2A.

3.2 Antarctica

Overlapping ERS-2 and NSCAT data are shown for the second half of September in Fig. 4, to illustrate the corresponding C- and Ku-band austral spring ice sheet responses. This period is prior to the summer melt and illustrates the typical winter ice-sheet signature of Antarctica. Notably, there are a much broader range of backscatter variations than in Greenland. The simple pattern of relatively lower C-band backscatter in the central region of the ice sheet is clearly not reproduced as in Fig. 3, and the ice sheet facies are limited to simply dry snow and percolation zone. High snow accumulation regions (> 200 kg m^{-2} a^{-1}) around the peripheral slopes of the ice sheet, particularly in Wilkes Land in East Antarctica, and Ellsworth Land and Marie Byrd Land, have typically low EScat and NSCAT *A* values, together with relatively lower NSCAT *B* values (Fig. 4). For instance, accumulation values in the vicinity of Siple Station (75° 54'S 83° 54'W) are of the order of 550 kg m^{-2} a^{-1} [Ref. 12]. Further low *A* values are associated with high orographic precipitation along the western flank of the Antarctic peninsula [Ref. 13]. Despite low *A* values and high accumulation in some regions, EScat *B* values, appear locally sensitive to surface roughness and internal scattering effects, particularly around a number of volcanic peaks in Marie Byrd Land. Such interesting signatures are observed around Mount Takahe (76°15'S 112°W), Crary Mountains (76°45'S 118°W), Mount Hampton (76°29'S 125°48'W) in the Executive Committee Range, and the Ames Range (75°45'S 132°W), and are evident as saturated EScat *B* in Fig. 4c. The fact that NSCAT *A* values remain depressed around these volcanic peaks, despite high EScat *B* values, suggests that the effect is confined, however, to below the surface and is related to internal layering or buried crevasses only visible in more deeply penetrating, longer-wavelength, C-band data.

In Fig. 4, *A* images attain their highest values at both frequencies at high elevations in the central Antarctic ice sheet, in relatively low accumulation regions (< 100 kg m^{-2} a^{-1}). Strong layering in these regions promotes high *B* values (in Fig. 4c and d) and depth hoar development is thought to add a significant contribution to volume scattering totals in regions having NSCAT *A* values exceeding -2 dB. Depth hoar development is known to generate grain radii exceeding 0.5 cm in diameter in these regions through temperature-gradient metamorphism under strong vertical vapour fluxes. Large grains cause strong, wavelength-dependent Mie scattering at both Ku-band, and C-band rather than Rayleigh scattering. The result is an order of magnitude difference in *A* values, despite similar *B* values.

High *A* values are also observed in a number of lineaments and elongated features in the central part of the Antarctic ice sheet in the higher resolution NSCAT images. Several large ice streams flowing into the Ronne and Filchner ice shelves are identified in Fig. 4b, Inland extensions of the Slessor Glacier (79°30'S 24°W)

and southward trending tributaries of the Recovery Glacier (81°S 33°W) can be traced in the NSCAT data poleward of the of the EScat swath limit (with values exceeding -3 dB). Catchment areas are also visible for several large ice streams (Reedy, Scott and Amundsen Glaciers) flowing into the Ross ice shelf. These penetrate the Queen Maud Mountains into Ice Stream A, ultimately leading into the Ross Ice shelf. Blue ice regions, having a hard wind-swept, sublimating bare-ice surface also display high Ku-band values (10 dB higher than C-band), as for instance in the Queen Fabiola Mountains (72°S 36°E) in Queen Maud Land.

In contrast to Greenland, the Antarctic ice sheet experiences summer melting only at the lowest elevations around the coast. The percolation zone is limited to this geographic area in Antarctica. Melt events, although short-lived, are recorded in both

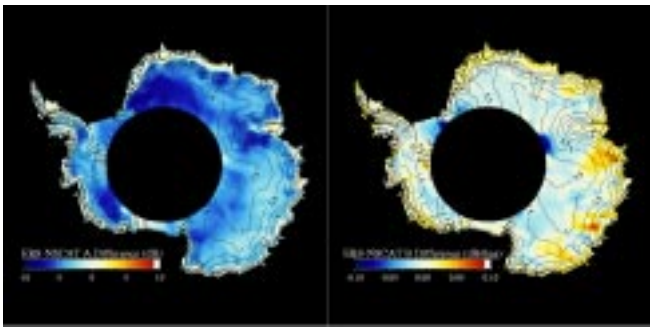

Figure 5. *Frequency difference images illustrating (a) ERS-2 - NSCAT A difference; and (b) ERS-2 - NSCAT B difference, for the time period shown in Fig. 4.*

NSCAT and EScat backscatter records as a dramatic summer depression in backscatter values due to snow wetting. The recent envelope of melt extent is clearly reflected in Fig. 4a as the halo of high coastal and ice shelf *A* values exceeding -5 dB, and in Fig. 6 as Δ*A* values close to 0 dB. As in Greenland the reason for the extremely high values is the formation of percolation features such as ice layers, lenses and glands in the firn. The resulting backscatter contrast between summer and winter months can exceed 20 dB, as in the case of the Larsen Ice Shelf (63°S 62°W).

Although limited in latitudinal extent by the EScat swath limit, the differences in Fig. 6 illustrate regions of frequency-dependent ice-sheet backscattering. Notable features which bear similarity to Greenland are the fringe of Δ*A* values where melting has its greatest impact. Recent intense melting on the Amery, Fimbul and Larsen ice shelves, for instance, leads to slightly positive differences, due to the greater penetration depth at C-band, and resulting higher volume scattering from buried ice lenses. Interestingly, the Ross ice shelf shows a large east-west gradient in Δ*A*. The eastern side of the ice shelf is known, for instance, to preferentially experience more cumulative melt days [Ref. 14] each year throughout the last decade, thereby building more ice lenses and layers.

The regions of the largest Δ*A* differences (< -5 dB) in West Antarctica (Fig. 5a) occur in Marie Byrd Land, and are confined to the region poleward of the Executive Committee Range. In East Antarctica a large portion of Queen Maud Land (with an extension into the Lambert Glacier drainage basin) and Antarctic Plateau regions poleward of 75°S have absolute *A* differences exceeding 5 dB. Since these areas correspond with regions of low azimuthal anisotropy [Ref. 15] and low accumulation rates (< 100 kg m^{-2} a^{-1}), it is suggested that wavelength-dependent differences result largely from the frequency of occurrence of depth hoar in the firn, and the effects of snow grain volume scatter.

Frequency difference *B* image values in Fig. 5b show relatively uniform near-zero values throughout central Antarctica, indicating the negligible contribution of surface roughness effects in these dry snow regions. The largest positive differences are confined close to the coast in the percolation zone, and further inland in regions of intense, persistent katabatic winds. Examples may be found in Enderby Land near Mizuho Station (71°20'S 46°30'E), and in other regions where the erosion environment prevents high accumulation such as Princess Elizabeth Land (70°S 90°E), Wilkes Land (70°S 123°E), and George V Land (70°S 140°E). Not coincidentally, these regions display the highest azimuthal anisotropy [Ref. 15], and estimates of *A* and *B*, using equation (1), are susceptible to a high degree of variance. Nevertheless, the positive Δ*B* values suggest a significant influence from wind-induced, erosional surface-roughness features such as sastrugi, and cross-bedding caused by seasonal erosion and uneven accumulation.

4. DECADAL CHANGE

Acquisition of NSCAT data during the same September season as Seasat, enabled long-term, 1996-1978 change maps to be derived over both ice sheets in late September. In Greenland, this period corresponds with late autumnal cooling over the ice sheet, while in Antarctica it corresponds with the austral spring. Since melting may influence a large portion of the Greenland ice sheet, change is primarily influenced by diagenetic changes resulting from snow-surface melt. However, since most of Antarctica may be regarded as a 'dry-snow' zone, changes result not from the effects of positive summertime air temperatures. Rather these changes express the effects of net, long-term variations in snow accumulation and thus layering in the snowpack, or significant dynamic adjustments of the ice sheet, expressed as large-scale surface roughness changes. The results shown in Fig. 3c and Fig. 6, illustrate the decadal time-scale changes on the Greenland and Antarctic ice sheets, respectively.

4.1 Greenland

Subtle differences in σ°_{vv} (*i.e.* NSCAT-SASS) between Fig. 3a and b are shown in Fig 3c, (where Fig. 3b is the result of combining and median filtering the relatively sparse SASS measurements). Surfaces experiencing large changes over the intervening 18 year period are in Fig. 3c noted as dark tones with values > -3 dB. Patterns appear highly correlated with the snow and ice facies boundaries in Fig. 2a. and the zones of largest interannual variability. The upslope melt extent has a large interannual variability and the mean July melt area in Fig. 2 clearly does not capture the maximum extent of melting often experienced within a narrow range of dates. Fig. 3c therefore contains microwave radar

archaeological evidence for previous melting within the dry snow zone, through the influence of buried scatterers beneath recent years of snow accumulation. Patterns suggest a recent upslope migration of the upper boundary of the percolation zone, particularly in response to the extreme summer of 1995 (in Fig. 2e). NSCAT probably penetrates deep enough to 'see' percolation inhomogeneities formed along the lower elevation fringes of the dry snow zone, and the frequency difference image in Fig. 3e corroborates these changes. Fig. 3e highlights zones of wavelength-dependent volume scattering. As dry snow has a lower σ° at C-band, due to the primary backscattering occurring from Rayleigh scattering from snow grains (in the absence of strong stratigraphy), this zone has large positive values > 8 dB in Fig. 3e. A contrast reversal occurs in the zone influenced by percolation, due to EScat penetrating deeper and responding more to buried ice lenses than NSCAT. This results in slightly negative percolation zone values.

Lower accumulation rates result in more pronounced stratification, and greater backscattering from subsurface layers at high incidence angles. This is particularly true for instance in the north-east Greenland dry-snow zone, and is seen in SASS data [Ref. 5]. Thus, we suggest that time series of multiple frequency, enhanced resolution *A* images and their associated *B* values, together offer greater potential for retrieving snow accumulation than single channel, fixed incidence angle instrument data.

4.2 Antarctica

Decadal differences of the kind illustrated in Fig. 3b and Fig. 7 arguably suffer from the effects of interannual variability, particularly if seasonal variations in backscatter are large. Fig. 6 shows the recent past in the form of an interannual time-series spanning 1992-1997 in a region experiencing no melting, and expected constant forcing. The upper dotted line indicates a neutral long-term trend in passive microwave 19 GHz v-pol brightness temperatures which is suggestive of constant mean air temperatures. Nonetheless, a distinctive seasonal cycle is observed, with maximum temperatures in summer and minimum temperatures in winter and a dynamic range of ~20 K. Scatterometer measurements from both ERS-2 (crosses) and NSCAT (solid line) are anticorrelated with SSM/I, exhibiting ~ 0.5 dB amplitude in the seasonal cycle with peak backscatter values attained in August. The main conclusion from Fig. 6 is that the maximum error in decadal time-scale difference images, occurring

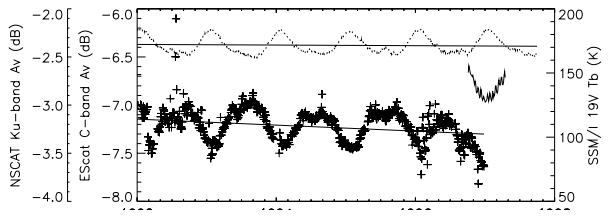

Figure 6. *Interannual time series indicating Antarctic plateau (78°S 122°30'E) mean v-pol EScat and NSCAT A values, and corresponding 19GHz v-pol SSM/I brightness temperatures, for the period 1992 – 1997.*

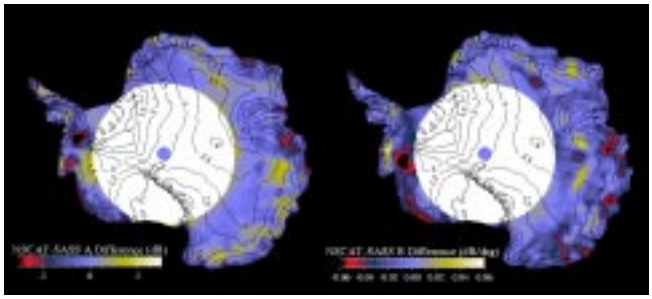

Figure 7. *NSCAT–SASS A and B difference images for the same 23-28 September 6-day period in 1996 and 1978, respectively.*

as a result of interannual variations in the seasonal cycle is of the order of 0.5 dB for ice-sheet surfaces experiencing no melt.

Fig. 7 shows the 18-year *A* and *B* differences (v-pol), computed between late September images acquired during the SASS and NSCAT missions. Excluding ice shelf regions, in some cases of which the changes have been dramatic, there are a number of regions with 18-year reductions in Ku-band *A* values exceeding 2 dB and *B* values exceeding -0.5 dB/deg. In West Antarctica, the largest declines are observed in Ellsworth Land in the location of the Evans Ice Stream and the US "Eights" base (75° 20'S 77°W), and slightly north of the Pine Island Glacier (75°S 102°W). In this high accumulation region, an 18 year overall increase in annual accumulation is expected to have had a significant impact on the snow density and layer thickness, together with the mean grain radius. It is speculated at present that the resulting increases in layer spacing and fraction of lower density snow, have caused a decrease in *A* and *B* values at these elevations. This area of corresponding *A* and *B* decreases may be tracked westwards around Ellsworth Land between the 1000 and 1500m elevation contours. Both below and upslope of this broad region, *A* differences become positive, suggesting large spatial gradients in changes over the last 20 years, and that the West Antarctic increase in accumulation occurred at a distinctive elevation. This suggests a combination of orographic and adiabatic influences upon changes precipitation patterns.

In East Antarctica a further significant-sized region of negative ΔA and ΔB values occurs in Princess Elizabeth Land at 70°S 85°E. This correspondence between reductions in *A* and *B* values similarly implies a snow accumulation increase, albeit within a broader range of elevations between 1000 to 3000m. Other centers of positive ΔA values of 1–2dB are dispersed throughout East Antarctica. Further analysis is required to examine whether these changes are a response to accumulation changes or long-term variations in the katabatic wind regime.

5. CONCLUSIONS

Scatterometers clearly provide important information about the large ice sheets. This precisely calibrated spatial and temporal record is complementary to passive microwave images from SSM/I and snap-shot images produced by higher resolution radar sensors such as SAR. Time series of images with large-area coverage, such as that shown here, are suitable for monitoring

changes in the characteristic zones of ice sheets in response to changes in accumulation, metamorphism and melting. Significant 18 year differences between early NSCAT and Seasat SASS images indicate large-scale changes in radar backscatter in response to changing snow and ice surface conditions.

Frequency combinations and the addition of passive microwave emission data from SSM/I help compensate for the wavelength-dependent scattering albedo of the snow and the high incidence angle component of volume backscatter caused by snow grains, as opposed to the stratification induced scattering. This allows dependencies of the backscattering on snow density, temperature, ice particle radius and layer depth to be better parameterized. In this manner, algorithms are presently being developed to monitor the seasonal progression of snow accumulation and firnification using combined frequency scatterometer and passive microwave datasets. Future multi-channel, active-passive empirical algorithms developed along these lines will be invaluable for extending and testing current theoretical electromagnetic scattering models, and in validating our understanding of the physical basis for the observed microwave signatures.

Decadal variability in Greenland and Antarctica is forced primarily by the North Atlantic and El Niño Southern Oscillations, respectively. Regional impacts are greater than normal ablation and/or higher than normal snow accumulation. Greenland results indicate an upslope increase in the extent of the percolation zone and reduction in dry-snow extent since 1978, with the largest changes occurring in the south western flank of the ice sheet. This implies that the region of melting on the ice sheet has risen to its highest altitude in the recent past. Observations of the interannual variability show July 1995 was an extremely large melt season, probably the most significant over the 18 year interval since Seasat in 1978. Changes are consistent with the decadal warming trend and increase of more than 1.0^{o}C between 1979 and the present day in Greenland. In contrast, West Antarctic changes appear to suggest increases in snow accumulation have taken place. Such changes imply an increased poleward moisture flux in these regions.

6. ACKNOWLEDGEMENT

MRD completed this work at Jet Propulsion Laboratory, California Institute of Technology under contract to the National Aeronautics and Space Administration and supported by NASA Code YS and the NSCAT Project Office.

7. REFERENCES

1. Zwally H.J., A.C. Brenner, Growth of the Greenland Ice Sheet, *Science*, 246, 1587-1591, 1989.
2. Abdelati W., K. Steffen, Snowmelt on the Greenland Ice Sheet as Derived from Passive Microwave Satellite Data, *J. Climate*, 10(2), 165-175, 1997.
3. Rott H., Synthetic Aperture Radar Capabilities for Glacier Monitoring Demonstrated with Seasat SAR Data, *Z. fuer Gletscherkunde u. Glazialgeol.*, 16, 255-266, 1980.
4. Jezek, K.C., M.R. Drinkwater, J.P. Crawford, R. Bindschadler, R. Kwok, Analysis of synthetic aperture radar data collected over the southwestern Greenland ice sheet, *J. Glaciology*, 39, 131, 119-132, 1993.
5. Long D.G., M.R. Drinkwater, Greenland Observed at High Resolution by the Seasat-A Scatterometer, *J. Glaciology*, 32, 2, 213-230, 1994.
6. Benson C.S., Stratigraphic Studies in the Snow and Firn of the Greenland Ice Sheet, *CRREL Res Rep*., 70, Cold Regions Res. Eng. Lab., Hanover, NH, 120pp., 1962.
7. Rignot, E., Backscatter Model for the Unusual Radar Properties of the Greenland Ice Sheet, *J. Geophys. Res*., 100, E5, 9389-9400 , 1995.
8. Jezek, K.C., P. Gogineni, M. Shanableh, *Geophys. Res. Lett.*, 21, 1, 33-36, 1994.
9. Drinkwater M.R., D.G. Long, D.S. Early, *ESA Journal*, 17, 307-322, 1994.
10. Long, D.G., and M.R. Drinkwater, Cryosphere Applications of NSCAT Data, *IEEE Trans. Geosci. and Remote Sens*., In Press.
11. Early D.S., D.G. Long, Resolution Enhancement of Scatterometer Data, IEEE Trans. Geosci. Rem. Sens., In Press.
12. Mosley-Thompson, E., J. Dai, L.G. Thompson, P.M. Grootes, J.K. Arbogast, and J.F. Paskievitch, Glaciological Studies at Siple Station (Antarctica): Potential Ice-Core Paleoclimatic Record, *J. Glaciol.*, 37, 125, 11-22, 1991.
13. Giovinetto, M.B., and N.M. Waters, Dependence of Antarctic Surface Mass Balance on Temperature, Elevation, and Distance to Open Ocean, *J. Geophys. Res.*, 95, D4, 3517-3531, 1990.
14. Zwally, H.J., and S. Fiegles, Extent and Duration of Antarctic Surface Melt, *J. Glaciol*., 40, 463-476, 1994.
15. Early, D.S., and Long, D.G., Azimuthal Modulation of C-band Scatterometer σ^{o} over Southern Ocean Sea Ice, *IEEE Trans. Geosci. Rem. Sens.*, 35,5, 1997.